Stacking Sequence Dependent Photo-Electrocatalytic Performance of CVD Grown MoS2/Graphene van der…

Article *in* Nanotechnology · January 2017

DOI: 10.1088/1361-6528/aa565a

CITATIONS
0

READS
96

5 authors, including:

Ravi K. Biroju
TIFR- Center for Interdisciplinary Sciences, H…
21 PUBLICATIONS **59** CITATIONS
SEE PROFILE

Shubhadeep Pal
Tata Institute of Fundamental Research
5 PUBLICATIONS **6** CITATIONS
SEE PROFILE

Pravat K Giri
Indian Institute of Technology Guwahati
165 PUBLICATIONS **1,465** CITATIONS
SEE PROFILE

Tharangattu N Narayanan
TIFR Center for Interdisciplinary Sciences, TI…
117 PUBLICATIONS **1,941** CITATIONS
SEE PROFILE

Stacking sequence dependent photo-electrocatalytic performance of CVD grown MoS_2/graphene van der Waals solids

2017 Nanotechnology 28 085101

(http://iopscience.iop.org/0957-4484/28/8/085101)

IOP Publishing Nanotechnology
Nanotechnology 28 (2017) 085101 (12pp) doi:10.1088/1361-6528/aa565a

Stacking sequence dependent photo-electrocatalytic performance of CVD grown MoS_2/graphene van der Waals solids

Ravi K Biroju[1], Shubhadeep Pal[1], Rahul Sharma[1], P K Giri[2] and Tharangattu N Narayanan[1]

[1] TIFR-Center for Interdisciplinary Sciences (TCIS), Tata Institute of Fundamental Research, 21 Brundavan Colony, Narsingi, Hyderabad-500075, India
[2] Department of Physics and Centre for Nanotechnology, Indian Institute of Technology Guwahati, Guwahati-781039, India

E-mail: tnn@tifrh.res.in and tn_narayanan@yahoo.com

Received 27 October 2016, revised 16 December 2016
Accepted for publication 3 January 2017
Published 23 January 2017

Abstract

New layered solids by the combinatorial stacking of different atomic layers are emanating as novel candidates for energy efficient devices. Here, sequentially stacked single layer graphene-molybdenum disulfide (MoS_2) van der Waals (vdW) solids are demonstrated for their efficacy in the catalysis of hydrogen evolution reaction (HER), and importance of their stacking order in tuning the photo-electrocatalytic (PEC) efficiency is unraveled. Single layer graphene and a few layered MoS_2 stacked vdW solids based transparent flexible electrodes were prepared, and a particular stacking sequence where top-graphene: bottom-MoS_2/polydimethylsiloxane (PDMS) geometry (MSGR) exhibited the lowest onset and over potentials and a very high exchange current density ($j_0 \sim 245 \pm 1\ \mu A\ cm^{-2}$) in acidic HER in comparison to the individual layers and other stacked configuration (MoS_2 on top of graphene on PDMS, GRMS). The HER studies under dark and white light illuminations were conducted to explore the PEC responses of the devices. The augmented HER performance of MSGR is further confirmed from the charge transfer resistance measurements using electrochemical impedance spectroscopy. Role of graphene plasmonics and MoS_2 to graphene electron transfer were studied, and this study unravels the importance of a new factor, stacking order of vdW layers, while designing novel devices from the layered solids.

Supplementary material for this article is available online

Keywords: photo-electrocatalysis, graphene, MoS_2

(Some figures may appear in colour only in the online journal)

1. Introduction

Engineering of atomic (two-dimensional (2D)) layers is receiving immense attention from the scientific community due to the possibilities of tuning the optical, mechanical, electronic and electrochemical properties of individual layers to make them amenable for energy and environmental applications [1, 2]. Molybdenum disulphide (MoS_2) is one of the largely investigated 2D materials, where its physico-chemical properties show a drastic contrast in comparison to its bulk [3]. Visible light absorption, indirect to direct bandgap transition, layer dependent photoluminescence (PL) etc are some of the stark contrasts in atomically layered MoS_2 sheets from bulk, making them unique for photocatalysis and photo-electro catalysis (PEC) [4–6] applications.

Apart from the in-plane engineering of atomic layers by dopants, out of plane staking of in-plane bond saturated layers resulting in to van der Waals (vdW) solids is identified as a strategic route for the development of new functional atomic layers/solids [7, 8]. Our group recently demonstrated the

formation of interface induced dipoles in the vdW stacks of graphene and boron nitride, and tunability in the photoconductivity of these macroscopic solids by engineering their interfaces [9]. Similarly, plasmon-enhanced strong visible light photocatalysis from defect engineered chemical vapor deposited (CVD) graphene and gold substrate induced enhanced electrocatalytic activities of boron nitride are recently reported by different groups [10, 11]. It has also been established that the underlying substrate and its defects can influence the spin and charge density distributions of atomic layers, similar to that of a heteroatom doping in graphene [12]. These modifications can influence the catalytic activities of atomic layers. Recent density functional theory based studies showed that the existence of graphene layer below the MoS_2 layer has a noticeable influence on the charge density distribution of MoS_2 layers [12]. It has been shown that the built in electric field in MoS_2/graphene hybrid forms an excessive negative charge density in the structure, which eventually enhances the hydrogen evolution reaction (HER), one of the purest methods to generate H_2—a renewable energy source. Further, such a sandwich structure can also make the basal plane of MoS_2 close to the thermo-neutral (adsorption–desorption energy difference $\Delta G \sim 0$), enabling the basal plane to be active towards the HER, which is otherwise inactive towards the reaction [12].

Edge sites of large surface area MoS_2 with Mo and S atoms (2H and 1T phase) terminations play a crucial role in providing high adsorption kinetics of H^+ ions reduction reaction, where adsorption is the rate determining step in this multi-step process [4]. The authors group have reported that edge state manipulation by size variation can tune the catalytic activities of MoS_2 [13]. Kong *et al* have shown that the enhanced activity of MoS_2 towards the HER can be realized by vertical alignment of sheets by laborious patterning process [14]. High quality crystals of single layer MoS_2 can be grown using chemical vapor deposition and the triangle shaped crystals [15], the most commonly observed structure, on a graphene current collector can give high exchange current density in HER reaction [16]. The synergistic role of graphene as a current collector and MoS_2 basal plane activator will open a unique opportunity for MoS_2/graphene based HER catalysis. The high optical transparency and electronic conductivity of graphene can provide efficient current injection into the MoS_2 layers [17]. However, the lack of high crystalline quality metal dichalcogenides based heterostructures and the elastic deformation of layers during the layer by layer transfer and post transfer treatment processes hinder the development of vdW solids based high performance electrocatalysts and optoelectronic devices. Further, high quality crystals are also important in avoiding the recombination of photocarriers generated during the light exposure leading to a high current and low over potential for the reduction reaction studied here.

In the present work, high quality atomic layers of large area graphene (GR) and a few layered MoS_2(MS, 3–4 layers) were synthesized via a CVD method to form layer by layer assembled different sequentially stacked large area vdW solids. Two different vdW solids were realized on flexible polydimethylsiloxane (PDMS) substrates, namely top-graphene: bottom-MoS_2/PDMS geometry (MSGR) and top-MoS_2: bottom-graphene/PDMS geometry (GRMS). A systematic PEC study on the HER process of different electrodes, namely MS, GR, MSGR and GRMS is conducted and the importance of vdW stacking and its sequencing in HER catalytic activities are unraveled in this work, those are not explored in the literature. The role of surface in-homogeneity in MSGR towards the augmented HER process is also studied by micro-Raman studies.

2. Experimental

2.1. CVD growth of graphene

Large area (millimeter sized) monolayer graphene (SLGR) was synthesized using CVD on a Cu foil of thickness 25 μm (Alfa-Aesar). In the process, chemically cleaned Cu foil was inserted into a quartz chamber and flushed with Ar gas (300 standard cubic centimeters per minute (SCCM) for 5 min. Then, the chamber was pumped down to a base vacuum 4×10^{-4} mbar, and the temperature was increased to 1045 °C (growth temperature of SLGR) at a heating rate of 25 °C min^{-1} using a horizontal muffle furnace (Indfur, India). The Cu substrate was pre-annealed at the same temperature, in a reduced environment of H_2 gas maintained at a flow rate of 500 SCCM for 3 h in order to avoid oxidation of the Cu surface and increase the Cu grain size to get the complete coverage of graphene on the Cu foil. During the ramping and cooling, Ar: H_2 flow rate was kept at 300:20 SCCM. The final reaction was carried out by controlled flow of CH_4 in a flow rate of ~2 SCCM and $H_2 \sim 500$ SCCM for 15 min at 1045 °C. Since SLGR was deposited on both sides of the Cu foil, the bottom layer was removed by reactive oxygen plasma etching.

2.2. Transfer of graphene on to alien substrates

The SLGR on the Cu foil was transferred on to SiO_2/quartz/PDMS substrates by a conventional wet transfer technique [18]. In this process, a thin layer of poly(methyl methacrylate) (PMMA) in toluene (45 mg ml^{-1}) was spin coated on the Cu/SLGR layer and PMMA coated Cu/SLGR was kept for the drying at 150 °C for 15 min in a hot oven. The underlying Cu was etched using aqueous $Fe(NO_3)_3$ etchant solution. The SLGR/PMMA floating on the etchant solution was rinsed by deionized water for a few times, until the residual PMMA and metal impurities were removed. Then, it was scooped and transferred on to the required substrate manually. Further, it was kept in the oven for drying at 180 °C for 1 h. The graphene-PDMS substrates were heated on a hotplate at 100 °C for a few minutes until SLGR/PMMA is properly adhesive over the PDMS top surface. SLGR/PMMA was dipped in acetone for multiple times to remove the PMMA from the SLGR layers.

2.3. Controlled growth of a few layer MoS_2 using CVD

MoS_2 was directly grown on Si/SiO_2 and quartz substrates using a two zone quartz tube furnace based CVD system. In the procedure, MoO_3 (100 mg) and sulfur (S) powder (600 mg) were used as precursors. High-purity argon (Ar) gas was used as a carrier gas. S and MoO_3 precursors were kept in zone 1 and 2, respectively (supporting information, figure S1). SiO_2 and quartz substrates were inserted on the other end of the quartz tube in the zone 2. It may be mentioned that both S and MoO_3 precursors were separately loaded into two mini quartz tubes (inner diameter $\sim$ 10 mm) and kept at a distance 53 and 33 cm, respectively, from the substrates. This arrangement of precursors will provide a stable evaporation of S and MoO_3 sources by avoiding any cross-contaminations during the vapor transport and MoS_2 growth. The chamber was pumped down with a base pressure of 1.9×10^{-2} mbar and the temperature was increased to 600 °C at the rate of 17 °C min^{-1} for 45 min. During the ramping till 600 °C, Ar carrier flow was maintained at 50 SCCM keeping the pressure at 0.5 mbar and then increasing it slowly to 700 °C at the rate of 4 °C min^{-1} with 20 SCCM of Ar flow. The total time for MoS_2 growth was 50 min. During the first 10 min, the flow rate of the Ar was kept at 100 SCCM and later it was kept at 40 min, in order to have a controlled substrate temperature and stabilized vapor pressure. Furnace was cooled down to room temperature with the gas flow of 300 SCCM. The complete time line profile of the CVD grown few layer MoS_2 was shown in the supporting information, figure S1.

2.4. Fabrication of MoS_2-graphene vdW heterostructures

SLGR and MoS_2 based vdW heterostructures—MSGR and GRMS were developed by a wet transfer method. CVD grown SLGR was transferred directly on to the required substrate by the above mentioned PMMA based method and MoS_2 layers are transferred on to the graphene substrate by a mechanical transfer method in which MoS_2 containing Si/SiO_2 substrate was uniformly pressurized on the graphene containing substrate using a hydraulic pressurizer. This method was adopted for both the geometries. For, resonance Raman study, GRMS and MSGR samples were prepared on standard Si/SiO_2 (300 nm thick oxide layer) and PDMS substrates in order to evaluate the enhancement in the Raman signal of MoS_2 (E_{2g} and A_{1g} Raman modes, see supporting information) while electrochemical studies of individual layers and vdW heterostructures were conducted on conductive graphite ink (electrochemically inactive) pre-patterned (electrodes) PDMS substrate. A schematic representation of fabrication of vdW heterostructure for PEC performance studies is shown in figure 1.

3. Characterization

The morphology and microstructures of SLGR, MS, MSGR and GRMS were studied using a micro-Raman spectrometer and high resolution transmission electron microscope (HRTEM). Micro Raman measurements of pristine graphene and MoS_2 were performed with a high resolution commercial spectrometer (Horiba, LabRam HR), with excitation wavelength (λ_{ex}) 488 nm (Ar ion laser). Excitation source was focused with 100x objective lens, spot size 2 μm, laser power of 1 mW (to avoid the laser heating induced damage), and the signal was collected by a CCD in a back scattering geometry sent through a multimode fiber grating of 1800 grooves mm^{-1}. Resonance Raman measurements of vdW heterostructures were recorded with the confocal Raman spectrometer (Witech-Alpha 300 R and Renishaw Invia) using a single point acquisition (spectral resolution—0.5 cm^{-1}) at 488, 532 and 633 nm laser excitation having fine focusing with different objective lens magnifications 5x, 20x, 50x and 100x. HRTEM measurements were performed with a JEOL 2100 TEM at an operating voltage of 200 kV.

3.1. Photo-electrocatalysis measurements

A custom made electrochemical cell of standard three electrodes system was used for the PEC measurements, where the electrocatalytic measurement system consists of a high surface area spiral platinum wire as a counter electrode and silver/silver chloride (Ag/AgCl) (saturated KCl) as a reference electrode and a working electrode of SLGR/MS/their hybrids supported on a conductive graphitic pre-patterned contacts over the flexible PDMS substrates. A schematic of the visible light PEC system is shown in figure S2 (supporting information). A 300 W Xenon lamp source (Lelesil Innovative Systems, India) (wavelength range $\sim$370–730 nm) is used for the visible light excitation during electrochemical characterization of electrodes under light illumination. The three electrode electrocatalytic studies were carried out using a Bio Logic SP-300 electrochemical work station. Prior to the tests, the electrolyte (0.5 M H_2SO_4) saturated with N_2 flow for 30 min. Linear sweep voltammetry (LSV) was conducted at a scan rate of 10 mV s^{-1}. Electrochemical impedance spectroscopy (EIS) measurements were also performed in 0.5 M H_2SO_4. The working electrode was held at half- wave peak potential of the redox-probe over the frequency range 100 mHz–200 kHz at constant potential of -400 mV (RHE). The Chronoamperometric measurements in dark and light were performed on various electrodes to study the stability and visible light photo response/photocurrent characteristics at a constant potential.

4. Results and discussion

4.1. Micro-Raman and HRTEM studies

Figures 2(a), (b) show the optical microscope image of the CVD grown SLGR and MS, and the corresponding Raman spectra are shown in figures 2(c), (d). The Raman spectra of SLGR and MS were taken on Si/SiO_2 substrates, and the corresponding scanning locations are denoted by a red circular spot. Typical Raman fingerprints of SLGR—such as sharp G (1585 cm^{-1}) and 2D (2694 cm^{-1}) bands having

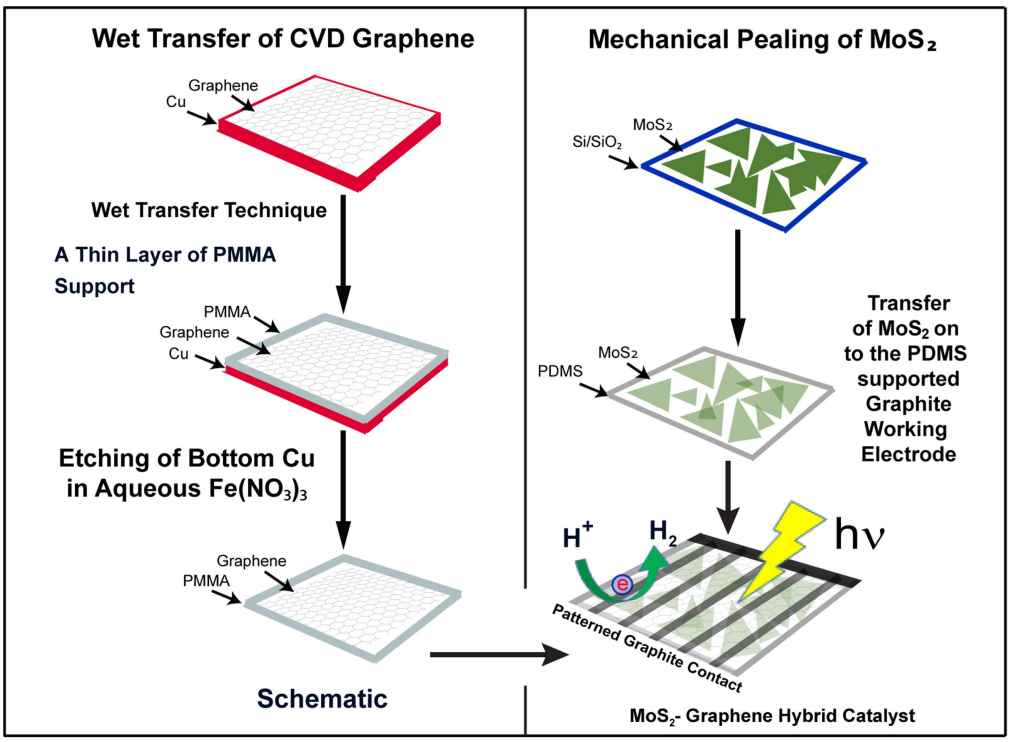

Figure 1. Schematic of the graphene transfer and fabrication of MoS_2-graphene van der Waals heterostructures on flexible PDMS substrates for the efficient visible light photo-electrocatalyst.

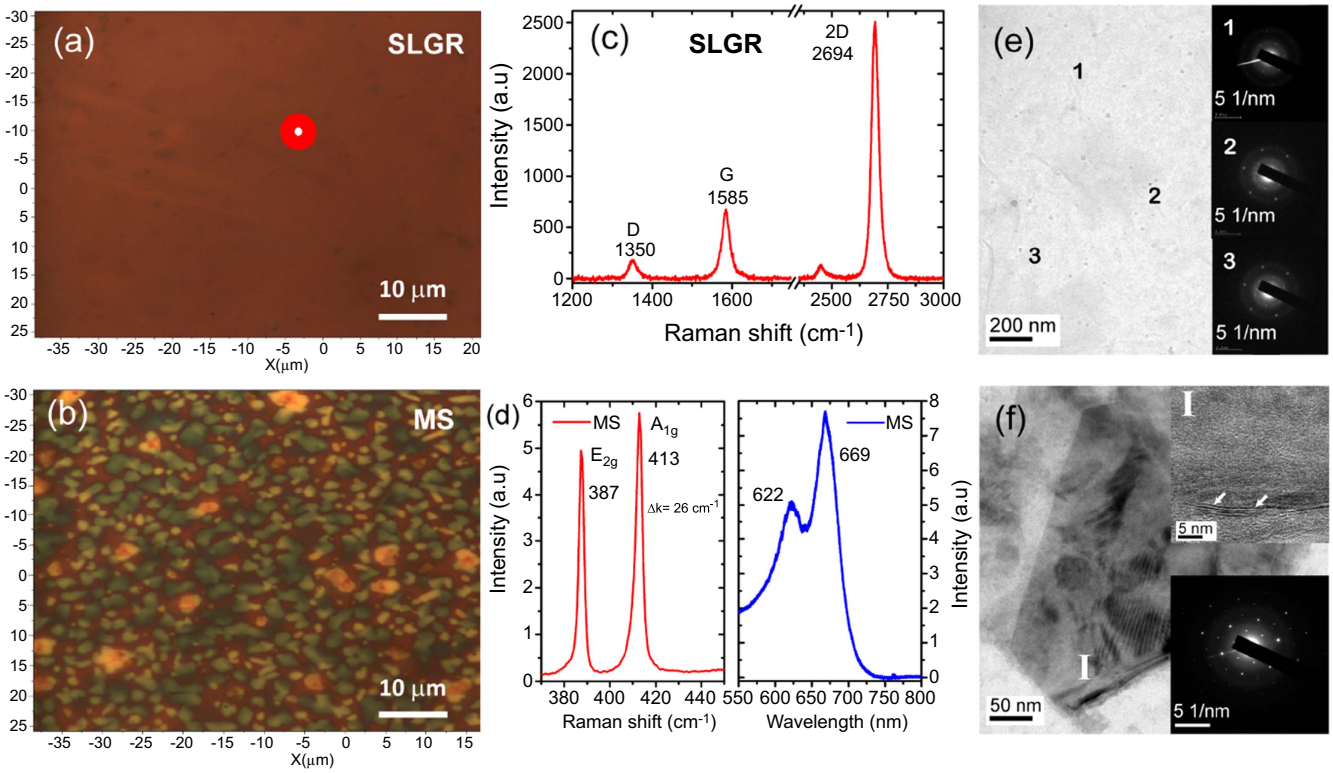

Figure 2. Optical microscope image of the CVD grown (a) large area single layer graphene (SLGR) and (b) a few layered MoS_2 on SiO_2 substrate. Typical Raman signatures of SLGR and a few layer MoS_2 are shown in (c) and (d), respectively. The photoluminescence (PL) spectra of a few layer MoS_2 is shown in the right panel of (d). The Raman/PL spectra is acquired with 488 nm laser excitation. (e) TEM image of the large area defect free SLGR and corresponding SAED patterns are significant for the SLGR large area coverage. The corresponding scanned locations of SAED are marked with serial numbers indicating the single layer hexagonal crystal structure. (f) TEM image of a single flake of a few layer MoS_2 transferred on to a TEM Cu grid. Top right inset corresponds to HRTEM image of a few layer MoS_2 focused at the region I and bottom right inset shows the SAED pattern of MoS_2 layers significant for the few layer coverage.

integrated intensity ratio of $I_{2D}/I_G \sim 4$, are shown in the figure 2(c). The full width at half maxima (FWHM) for both G and 2D bands are found to be ~23 and ~36 cm^{-1} respectively, indicating the presence of highly ordered defect free layer. However, a weak D band with very low intensity ratio $I_D/I_G \sim 0.3$ in the Raman spectra indicates the low level structural defects on the SLGR. Figure 2(d) represents the Raman spectra and visible photoluminescence (PL) spectra from a few layered MoS_2. CVD grown a few layered MoS_2 exhibits two important characteristic Raman modes at 387 and 413 cm^{-1}, which are attributed to E_{2g} and A_{1g} modes, respectively. The Δk represents the distance between the centers of the E_{2g} and A_{1g}, which reveals the number of MoS_2 layers [19]. In the present case, the average value of Δk estimated from the position dependent micro-Raman spectra is found to be ~26 cm^{-1} (see figure S4, Raman mappings of E_{2g}, A_{1g} bands including their area mapping), indicating the presence of 3–4 layers of MoS_2, which is consistent with HRTEM analysis (figure 2(f)). E_{2g} mode in MoS_2 is the in-plane vibration of two S atoms with respect to the Mo atoms, while the A_{1g} mode is associated with the out-of-plane vibration of only S atoms in opposite directions with respect to the Mo atoms. These two Raman modes are very sensitive to the local environment and surface impurities (defects) present on the atomic layers. The PL spectrum of MoS_2 layers (figure 2(d)) shows the strong PL bands at 622 and 669 nm, which are ascribed to 'B' exciton and 'A' exciton, respectively. 'A' excitation peak is derived from the direct band gap of MoS_2 and 'B' excitation peak arises from the direct gap transition between the minima of the conduction band and the lower level valence band maxima, where it is created by strong valence band spin–orbit splitting at the K point [20, 21]. Further the bandgap values matches exactly with the theoretical values indicating the absence of defects or strains on the as grown as samples and these studies on the individual layers indicate the crystallinity of the CVD grown MS layers.

Further, HRTEM images and selected area electron diffraction (SAED) patterns of SLGR are shown in figure 2(e), while figure 2(f) shows the TEM image of a few layer MoS_2 flake, and the corresponding lattice patterns of MoS_2 layers and its SAED are shown in the top right inset and bottom left inset, respectively. Electron microscopy studies show that the layered nature and hexagonal crystal structure (as revealed from the SAED pattern). The presence of graphene and MoS_2 layers on the SiO_2 and custom made PDMS flexible electrodes after transferring was characterized by micro-Raman spectroscopy. A high resolution field emission scanning electron microscope image of a MoS_2-graphene heterostructure (MoS_2 layers covered with a large area graphene, MSGR) is shown in figure S3 showing the large area coverage. Figures S4(a)–(b) (supporting information) show the Raman signatures of graphene and MoS_2, and corresponding optical microscopy images. Figures S4 (c)–(d) show the background corrected Raman spectra of the PEC devices indicating the presence of graphene and MoS_2. Figure S4(e) shows the Raman spectrum of the pristine MoS_2 after transferring it on to a PDMS substrate (luminescence from PDMS is evident in the spectrum), and figure S4(f) is the magnified portion of the same spectrum, which depicts the Raman signatures of MoS_2 layers ($E_{2g} \sim 380$ and $A_{1g} \sim 400$ cm^{-1}). These indicate that the successful transfer of layers to PDMS is achieved by the above mentioned process. Figure S5 shows the typical Raman spectra of the pristine MoS_2, which shows the broad line shape of E_{2g} and A_{1g} Raman modes and the corresponding Raman mappings of (b) E_{2g}, (c) A_{1g} and (c) Area under E_{2g} and A_{1g}. Raman spectroscopic imaging is performed over the as-grown MoS_2 on SiO_2 substrate, which is used to transfer MoS_2 layers onto flexible PDMS substrate. Note that the Raman mappings were recorded using 532 nm laser excitation in 5×5 μm^2 frame size.

4.2. HER studies

The HER performance and stability of various working electrodes (pristine and vdW layers of MoS_2 (MS) and SLGR (GR) made on PDMS) were investigated using three electrode LSV method and chronoamperometry, respectively. Note that both of the measurements were carried out in dark and visible light excitation conditions. All the measurements in dark and light were carried out in 0.5 M H_2SO_4 solution at a scan rate of 10 mV s^{-1}. Figure 3 shows the electrochemical HER activities (LSVs) of various samples. The corresponding Tafel slopes, estimated from the linear fit of on-set potential where the HER begins and logarithmic function of current density ($\log|J|$), are shown as insets. Further, comparison of HER activity of all the catalysts used in the present study with the benchmarked Pt/C catalyst is made in the supporting information (see figure S6), where Pt/C has a zero onset potential towards HER, as well cited by the researchers [13]. Chronoamperometry studies on pristine and MoS_2-graphene heterostructures are shown in figure S7, those are recorded at a constant potential (−0.4 V), where the HER is initiated in MSGR. In the case of MS, HER reaction starts at an onset potential of ~−0.45 V (versus RHE), above which the current increases drastically. This onset potential for MS is well in tune with other earlier reports [13, 22]. In the presence of light (LSV taken after 45 min of light exposure to the samples—MS_light), the onset potential shifts to a lower potential (~50 mV change) along with a drastic change in the current density. This indicates that photocarriers are being generated in MS after the exposure of light and they augment the reduction process of adsorbed proton. The SLGR electrode shows nominal HER response having an onset potential of ~0.55 mV with very low current density. It is important to note that the exposed light has little effect on SLGR, and neither the voltage nor the onset potential shifted after the exposure of light. The GRMS electrode (graphene at the bottom of MoS_2) shows similar onset potential as MS while the current density is drastically reduced. This indicates that the electron transfer in GRMS is not as efficient as in MS. The MSGR (graphene on the top of MoS_2) shows similar onset potential of MS in dark and but lower in light (~−0.35 V), while the current density of MSGR is drastically enhanced. Pristine MoS_2 has a reported over-potentials of −0.62 and −0.51 V (versus RHE), in dark and light, respectively, at 10 mA cm^{-2} [11]. Interestingly, in the present study MSGR

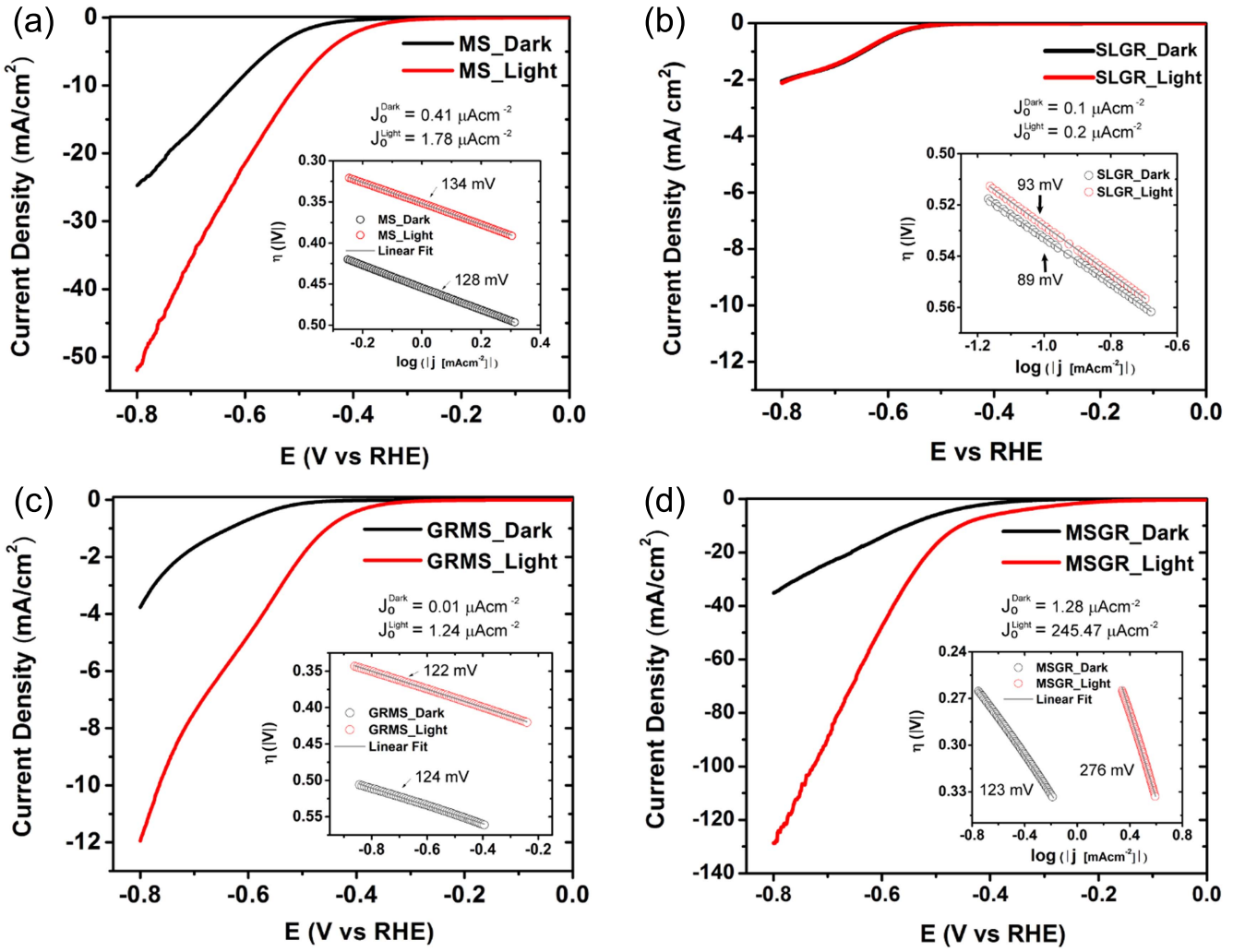

Figure 3. Polarization curves of the hydrogen evolution reaction (HER) in dark and light conditions in (a) pristine MoS_2 (MS), (b) pristine graphene (SLGR), (c) graphene-MoS_2 (GRMS) and (d) MoS_2-graphene (MSGR) vdW crystals. Note that the all the PEC devices are fabricated on the flexible PDMS substrates by the same procedure.

shows the lowest over potential having −0.45 V at 10 mA cm^{-2} in light. The stability performance of the MSGR is also found to be good, enabling it as a stable catalyst for HER as shown in figure S7.

MS, SLGR, and GRMS have almost the same Tafel slopes after light illumination, while in the case of MSGR it increased from 123 mV in dark to 276 mV in light. It has been reported that Tafel slope cannot give proper measure of kinetics in case of evolution reaction [23]. Similar thing can be observed in the case of MS and SLGR too. The exchange current density J_0 is one of the important parameters, which reflects the material's ability to exchange electrons from the working electrode to the counter electrode through the electrolyte solution at null potential, of various electrodes were calculated and are shown in the respective figures. Among the various electrodes (samples) studied here, MSGR showed the highest $J_0 \sim 245 \pm 1\ \mu A\ cm^{-2}$ during the visible light excitation. Exchange current density for the pristine MoS_2 is found to be 1.78 $\mu A\ cm^{-2}$, which is consistent with the reported values [13, 24]. In-addition, the chronoamperometric study on these samples are conducted and is shown in the supporting information, figure S7. Chronoamperometry is carried out at constant potential while monitoring the reaction current, which indicates the stability of the catalyst. In the case of CVD grown MoS_2-graphene samples, the potential is set at −0.4 V (versus RHE) where the HER will be just started (as inferred from LSV) in MSGR, and the same potential is kept for all the other samples too, as shown in the figure S7. MSGR catalyst shows a stability for more than 2 h. On the other hand, MS shows less current density, while in GR and GRMS, the current is very low due to their sluggish HER activity at this potential.

4.3. EIS studies

To further probe in to the HER performance of various samples, EIS measurements were performed on each samples in dark and light at −0.4 V (versus RHE) with sine wave having 10 mV amplitude, where the HER is supposed to be just initiated (onset potential). EIS is a power full technique, in which one can probe the heterogeneous electron transfer process. Figure 4 shows the Nyquist plots of pristine MS,

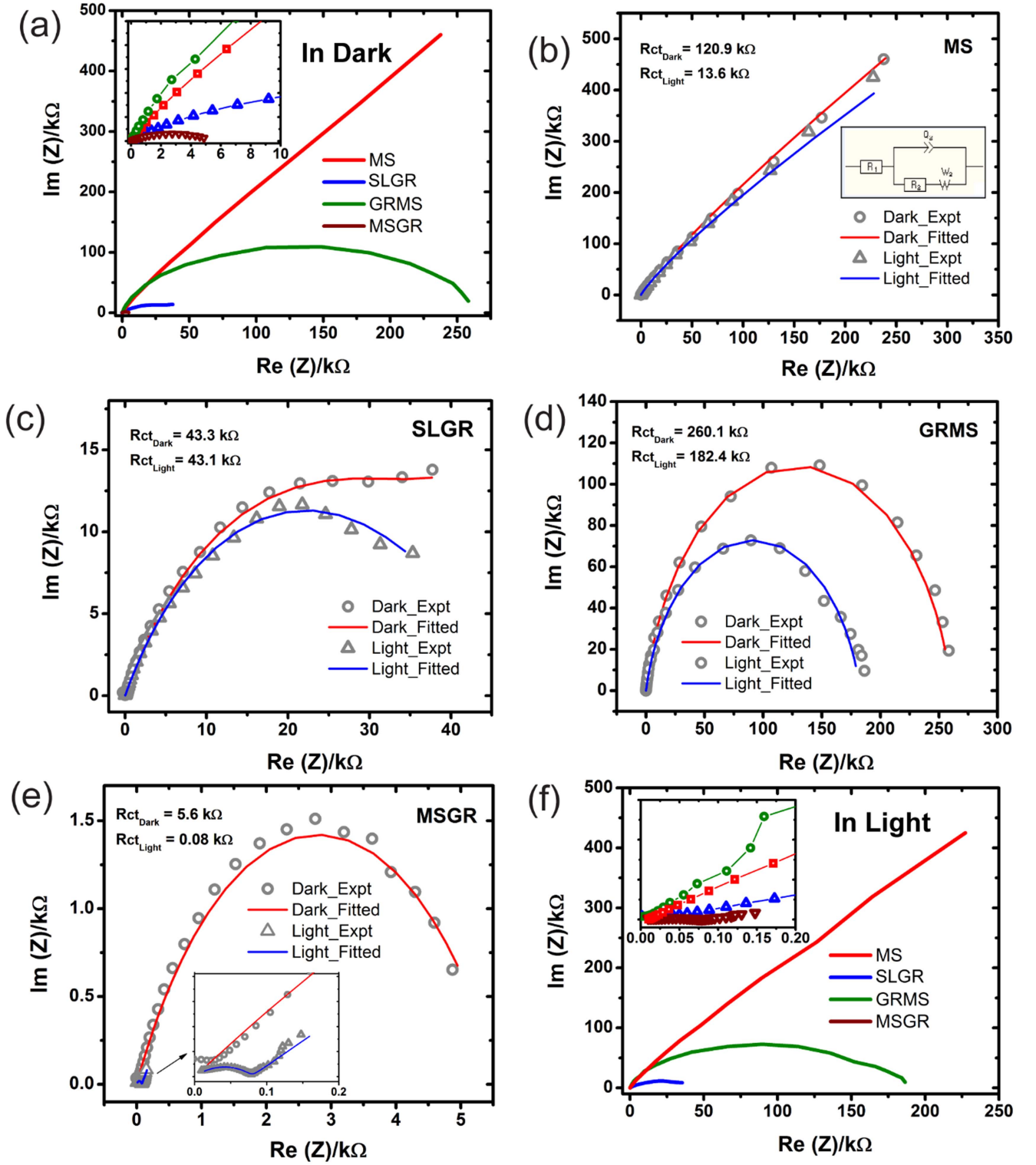

Figure 4. (a) Nyquist plots of pristine MoS_2 (MS), pristine graphene (SLGR), graphene-MoS_2 (GRMS) and MoS_2-graphene (MSGR) in dark. (b)–(e) Characteristic charge transfer resistance (R_{ct}) in (b) MS, (c) GR, (d) GRMS and (e) MSGR is estimated from the Randles circuit in dark and light conditions. Inset of the figure (e) shows magnified portion of the fitted data in MSGR. (f) Nyquist plots in MS, SLGR, GRMS and MSGR with the exposure of visible light. Insets of figures (a) and (f) represents the magnified portion of the impedance in the all the samples with dark and light. Note that all the measurements were performed in 0.5 M H_2SO_4 acidic electrolyte solution at constant potential (−400 mV versus RHE).

SLGR, GRMS and MSGR in dark. Inset shows the magnified view of the same. The charge transfer resistances (R_{ct}) of the individual samples are shown in figures 4(b)–(e), which are estimated from the Randles circuit in dark and light conditions (figure 4(b) (inset)). Randles circuit consists of solution resistance (R_1), charge transfer resistance (R_2 or R_{ct}), constant phase element (Q_2) and diffusion of ions in electrolyte solution represented by Warburg region (W_2). Among various samples, MSGR showed the lowest R_{ct} value in dark condition. Upon illumination, the R_{ct} value of MSGR is further reduced to 0.08 kΩ indicating the augmented charge transfer process in the presence of light. There is no considerable change in the R_{ct} values of SLGR upon illumination indicating the negligible effect of light on SLGR and this result is in tune with the LSV studies. The R_{ct} values of MS and GRMS were also decreased upon illumination, indicating the presence of light generated carriers in these electrodes. The EIS studies imply an augmented HER charge transfer process happening in MSGR and its response to the visible light in tune with the LSV studies.

4.4. Chronoamperometric photoresponse studies

In order to study the HER kinetics in various electrodes in the presence of light, chrono-amperometric photoresponse measurements (in 0.5 M H_2SO_4 medium) at −0.4 V (RHE) bias potential (a potential just below the onset potential in dark—to see the photoresponse of various electrodes) under dark and light exposure conditions were conducted. Figure 5(a) shows the comparison of photoresponse growth and decay profiles in the pristine and MoS_2-graphene hybrids recorded at the bias potential −0.4 V. The reaction currents in all the samples before light exposure are negligible or only residual current, and the reaction current after the light exposure can be assigned to the photogenerated carriers. SLGR did not show any photocarrier induced reaction current, while MSGR generated huge amount of current, higher than that of MS and GRMS after the exposure. It is also noted that though the enhancement in photocurrent is almost spontaneous (within 2–3 min after exposure) while the decay is delayed (∼25 min) after switching off the light source before it gets exponentially decayed. This slow enhancement in current in the initial exposure time is in tune with the shift in the onset potential observed in MSGR in LSV measurements (hence the observed slow increase in the current in LSV of MSGR after light exposure is not due to residual current). The experimental results (J_0 and R_{ct} values of SLGR, MS, GRMS and MSGR in light on/off conditions) are summarized in the figures 5(b) and (c).

Based on the above observations, a mechanism for the observed light activated HER process is proposed, and it is presented in figures 5(d)–(g), theoretical studies on this aspect are ongoing. SLGR has negligible photo generated carriers, where ∼98% visible light transmittance is theoretically predicted for SLGR. The samples containing MoS_2 has considerable photocurrents as observed in the chronoamperometry. The photogenerated carriers can be used for proton reduction (as shown in figure 5) and hence photocatalytic H_2 production can happen in MoS_2 containing samples. But the current collection efficiency of various geometries (electrodes/samples) discussed here are different. In the case of MS, most of H^+ adsorption centers will be at the edges of the top surface of the electrode. The small triangle shaped MoS_2 sheets are disconnected and distributed over the SLGR/graphite patterned electrodes (as inferred from figure 2(b)). This maybe the reason for the delayed photocarrier activities (growth and decay) in MS, MSGR and GRMS. The GRMS also generates photocarriers and then the HER reaction takes place. However, in this geometry, carriers find more barriers and resistance to participate in electrochemical reactions, since generated carriers are mobile through the bottom graphene and cross the MoS_2 barrier to reduce proton, which is absorbed at the top surface of the active sites of MoS_2. Thus, the MSGR configuration turned out as the best geometry to exhibit high amount of generated carriers and its effective transfer to the large area active sites of MoS_2 through the conductive graphene platform. The strains and ripples produced on graphene due to the underlying irregular MoS_2 triangle patches can also introduce additional H^+ adsorption sites at graphene. To probe the effects of graphene ripples and plasmonic effects in MSGR, a detailed micro-Raman study was conducted.

4.5. Resonance Raman and photoluminescence (PL) studies

To understand the roles of in-plane strain, ripples (surface inhomogeneity) and charge transfer in graphene-MoS_2 structures, point Raman spectra/mappings (the points are mentioned in figure 6(a)) and PL measurements of MS upon Raman excitation as shown in figure 2(d) (emissions at 622 and 669 nm) were conducted on MSGR and GRMS electrodes using four different objective lenses—5x, 20x, 50x and 100x, having numerical apertures (NA) of 0.12, 0.4, 0.55, and 1.25, respectively. Figure 6 (as well as figure S8) shows the point Raman mappings and PL spectra scanned for various spots in the MSGR sample. Here, points 1, 2 and 5 represent the edges of MoS_2-graphene interface in MSGR (refer to figures 6 and S8(d)), points 3, 4, 6, and 7 represent middle portions of MoS_2-graphene interface in MSGR and point 8 represents MoS_2 alone. Figures 6(a)–(d) represents Raman mappings of E_{2g} (382 cm^{-1}) and A_{1g} (407 cm^{-1}) modes of MoS_2, and G-band (1590 cm^{-1}) and 2D-band (2690 cm^{-1}) of graphene in MSGR. The intensity profile for each band at the corresponding locations are shown in the color bar indicated by the vertical scale. The Raman/PL spectrum (PL bands at ∼630 and 680 nm (broad humps) corresponding to the Raman excitation at 532 nm) for each spot is shown in the figure 6(e). Figure 6(f) represents the objective lens dependent Raman spectra in MSGR sample, which is recorded with 633 nm laser excitation.

It is noted that the intensity of PL spectra (broad PL spectrum) at point 6 (MoS_2-graphene) is higher than that of point 8 (pristine MoS_2). Further, Raman intensities of E_{2g} and A_{1g} are also enhanced in MSGR than MS in SiO_2 substrate (figures S5(a)–(e), 488 nm excitation). This enhancement in Raman and PL intensities of MoS_2 in MSGR can be due to

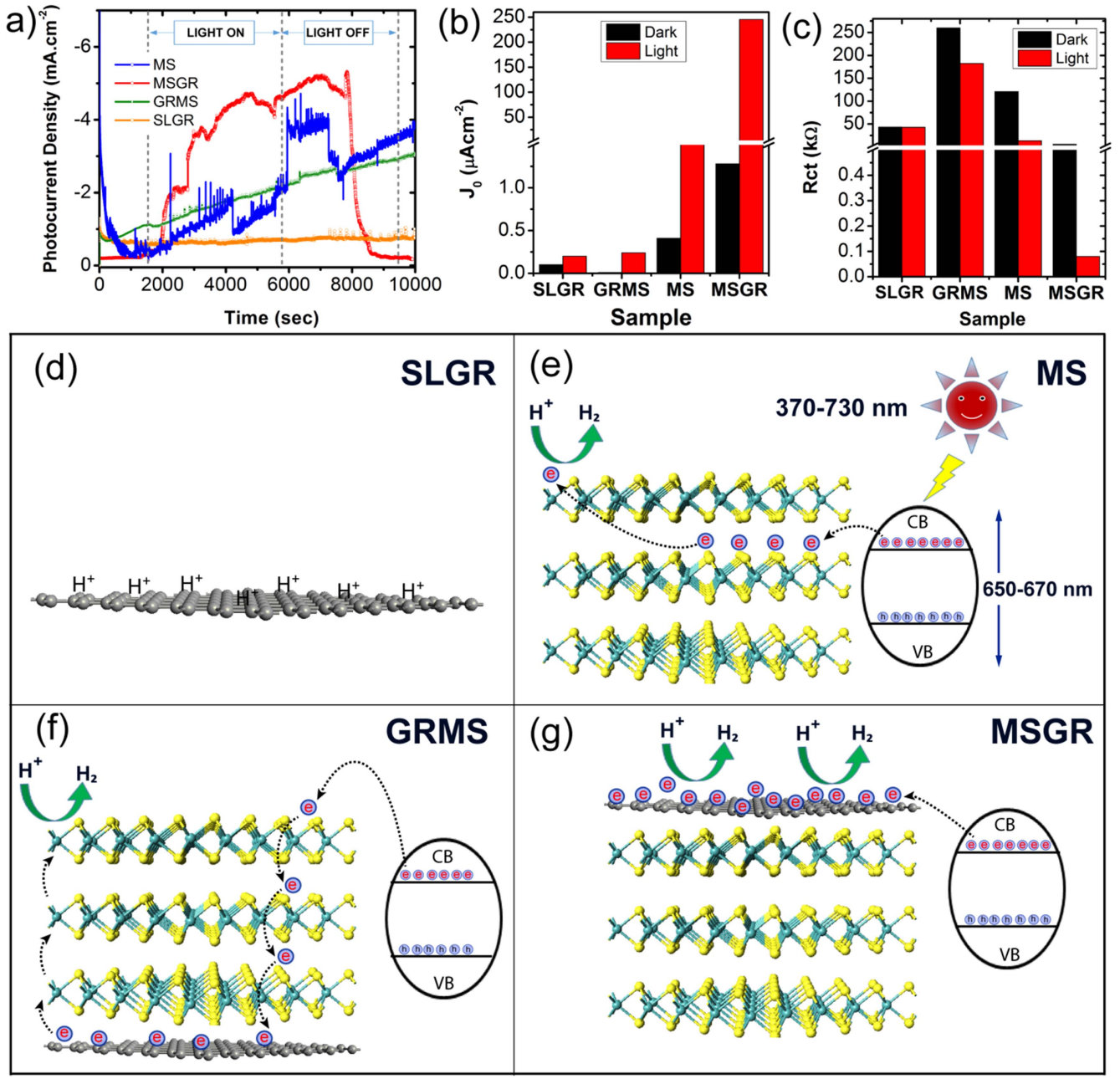

Figure 5. (a) Chronoamperometric photocurrent characteristics of pristine and MoS_2-graphene vdW hybrids with different stacking sequence measured at the bias potential (a) −0.4 V. Bar diagrams show the (b) comparison of exchange current density (j_0) and (c) charge transfer resistance (R_{ct}) in pristine and hybrids of MoS_2 and graphene in dark and light. (d) Mechanism of Stacking sequence dependent enhanced visible light photoelectrocatalytic activity in MoS_2-graphene vdW hybrids.

the presence of top-graphene (SLGR) in MSGR [25, 26]. However, the 2D band intensity of SLGR in SLGR-SiO_2 is higher than SLGR in MSGR indicating the effects of strains and ripples of graphene in MSGR due to the presence of bottom patchy, triangle MoS_2 sheets (figure 1, schematic). The PL enhancement of MoS_2 in MSGR is further compared in figure S8(f) (figure S8 is on Si/SiO_2 substrate and figures S9(c) and (d) on PDMS substrate), where the PL spectrum is recorded using two different objective lenses (20X and 100X). This indicates that at different NA values, the intensities of MSGR is much higher than MS. Further, the PL enhancement and red shift in the A exciton peak of MS in MSGR also indicate the photo-excited charge transfer from MoS_2 to graphene during Raman measurements [27–29]. The Resonance Raman scattering from MSGR in PDMS (similar to Si/SiO_2) substrate is observed and is shown in figure S9(c) (633 nm). This rules out the chances of PDMS substrate induced effects in Raman measurements. Surface in-homogeneity in graphene at MSGR causes strain induced D bands in graphene (as observed in figures 6, S9(b)–(d) and they may introduce additional H^+ adsorption centers at graphene. A detailed electrochemical scanning tunneling spectroscopy study is needed to map these adsorption centers, and these studies are under progress.

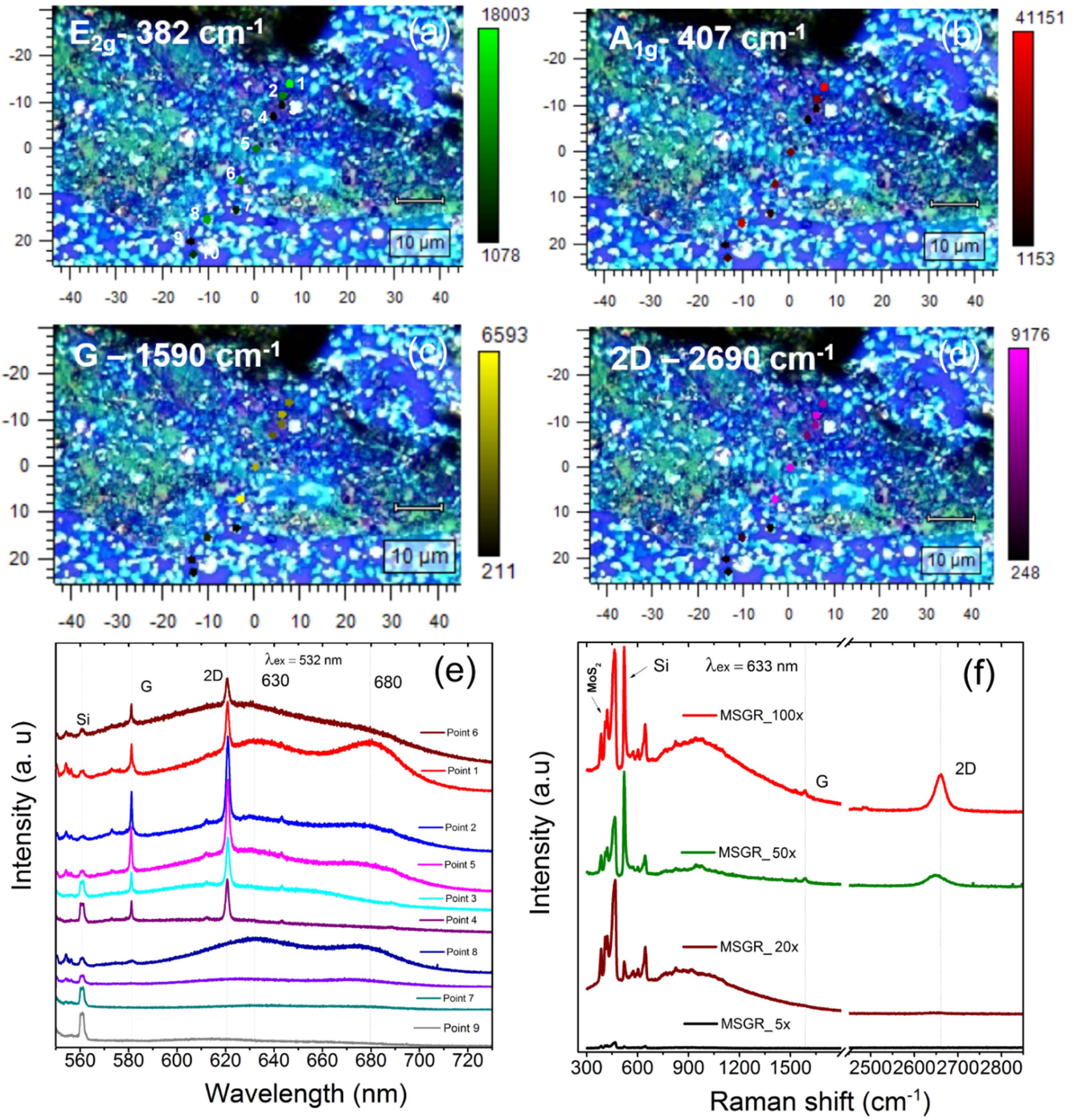

Figure 6. Raman mappings of (a) E_{2g}, (b) A_{1g}, (c) G and (d) 2D bands in MoS_2-graphene (MSGR) heterostructure. (e) Micro- Raman and photoluminescence (PL) spectra of MSGR sample recorded at different positions as shown in the figure. Note that the corresponding intensity profiles are labeled at the scanned locations with serial numbers as shown in the figure (a). (f) Raman spectra of MSGR recorded with different numerical objective lenses. Note that the Raman/PL mappings were recorded with excitation wavelength—532 nm having the spot size of 1 μm.

To study the substrate induced Raman effects of MS and SLGR, similar Raman studies were conducted on GRMS. However, graphene induced enhanced Raman signatures of MoS_2 were not observed in GRMS, figure S9(a), where graphene acts as a current collector and its presence may modify the potential of the adjacent MoS_2 layers [12]. It has been recently shown that work function of MoS_2 is higher than that of graphene and hence the electrons will move from MoS_2 to graphene [12]. Hence, the built in electric field will help for an augmented charge transfer between graphene and MoS_2, and also will help for the formation of additional H^+ adsorption centers (metallic centers by strain) on graphene. Electron transfer mainly happens between the immediate graphene-MoS_2 layers, while the MoS_2 layers further away from graphene are unscathed [12]. Hence graphene on top will modify the charge transfer between top MoS_2 (those

layers active towards catalysis) and graphene layers, acts as a current collector, and also can modify the surface by substrate induced strain and doping effects (formation of metallic centers). Further, metal dichalcogenides are questioned for their long stability upon exposure to the environment, and top graphene based MSGR can overcome this issue due to the coverage of SLGR over MS.

5. Conclusion

CVD grown single layer graphene and three-four layered MoS_2 atomic layers based electrodes were constructed by simple transfer techniques, and the van der Waal stacking sequence dependency of the stacked hybrids in the HER catalytic activities is tested. Graphene on top of the few layered MoS_2 (MSGR) showed highest HER activity in comparison to the individual layers and MoS_2 on top of graphene (GRMS) structure. The augmented HER charge transfer properties of MSGR were confirmed by charge transfer measurements, where the lowest charge transfer resistance is observed for MSGR. The exchange current density of MSGR was found to be enormously higher ($245 \pm 1\ \mu A\ cm^{-2}$) than other geometries and the reported values. Synergistic effects of graphene as current collector, plasmonic support, proton adsorption center and surface protective layer for MoS_2 based devices can open new avenues for van der Waals solids based photo-detectors and energy devices. This study establishes the important of a new factor, van der Waals stacking sequence, while developing atomic layers based electrocatalysts and charge transfer systems by the 'mix and match' of various layers.

Acknowledgments

Authors acknowledge the TCIS for financial support. Authors also thank Ms Larionette P L Mawlong and Mr Jitendra Kumar (IIT Guwahati) for helping in Raman measurements and simulation of graphene and MoS_2 atomic models using the ATK toolkit, respectively. Authors acknowledge Dr Kiran K Tadi (Presently at Hebrew University) and Mr Kapil Bhorkar (Presently at Nanyang Technological University, Singapore), TCIS for their assistance in some part of this work. The authors acknowledge IIT Guwahati for providing a HETEM facility.

References

[1] Geim A K and Grigorieva I V 2013 Van der Waals heterostructures *Nature* **499** 419
[2] Britnell L *et al* 2013 Strong light–matter interactions in heterostructures of atomically thin films *Science* **340** 1311
[3] Xu M, Liang T, Shi M and Chen H 2013 Graphene-like two-dimensional materials *Chem. Rev.* **113** 3766
[4] Velicky M, Bissett M A, Woods C R, Toth P S, Georgiou T, Kinloch I A, Novoselov K and Dryfe R A W 2016 Photoelectrochemistry of pristine mono- and few-layer MoS_2 *Nano Lett.* **16** 2023
[5] Merki D and Hu X 2011 Recent developments of molybdenum and tungsten sulfides as hydrogen evolution catalysts *Energy Environ. Sci.* **4** 3878
[6] Laursen A B, Kegnaes S, Dahl S and Chorkendorff I 2012 Molybdenum sulfides-efficient and viable materials for electro—and photoelectrocatalytic hydrogen evolution *Energy Environ. Sci.* **5** 5577
[7] Gao G *et al* 2012 Artificially stacked atomic layers: toward new van der Waals solids *Nano Lett.* **12** 3518
[8] Song L, Liu Z, Reddy A L M, Narayanan N T, Taha-Tijerina J, Peng J, Gao G, Lou J, Vajtai R and Ajayan P M 2012 Binary and ternary atomic layers built from carbon, boron, and nitrogen *Adv. Mater.* **24** 4878
[9] Krishna M B M *et al* 2015 Engineering photophenomena in large, 3D structures composed of self-assembled van der Waals heterostructure flakes *Adv. Opt. Mater.* **3** 1551
[10] Biroju R K, Choudhury B and Giri P K 2016 Plasmon enhanced strong visible light photocatalysis by defect engineered CVD graphene and graphene oxide physically functionalized with Au nanoparticles *Catal. Sci. Technol.* **6** 7101
[11] Kohei Uosaki G E, Noguchi H, Masuda T, Lyalin A, Nakayama A and Taketsugu T 2014 Boron nitride nanosheet on gold as an electrocatalyst for oxygen reduction reaction: theoretical suggestion and experimental proof *J. Am. Chem. Soc.* **136** 6542
[12] Honglin Li K Y, Li C, Tang Z, Guo B, Lei X, Fu H and Zhu Z 2015 Charge-transfer induced high efficient hydrogen evolution of MoS_2/graphene cocatalyst *Sci. Rep.* **5** 18730
[13] Pal S, Tadi K K, Sudeep P M, Radhakrishnan S and Narayanan T N 2017 Temperature assisted shear exfoliation of layered crystals for the large-scale synthesis of catalytically active luminescent quantum dots *Mater. Chem. Front* (https://doi.org/10.1039/C6QM00081A)
[14] Kong D, Wang H, Cha J J, Pasta M, Koski K J, Yao J and Cui Y 2013 Synthesis of MoS_2 and $MoSe_2$ films with vertically aligned layers *Nano Lett.* **13** 1341
[15] Ananth Govind Rajan J H W, Blankschtein D and Strano M S 2016 Generalized mechanistic model for the chemical vapor deposition of 2D transition metal dichalcogenide monolayers *ACS Nano* **10** 4330
[16] Behranginia A *et al* 2016 Highly efficient hydrogen evolution reaction using crystalline layered three-dimensional molybdenum disulfides grown on graphene film *Chem. Mater.* **28** 549
[17] Lee J M, Yi J, Lee W W, Jeong H Y, Jung T, Kim Y and Park W I 2012 ZnO nanorods-graphene hybrid structures for enhanced current spreading and light extraction in GaN-based light emitting diodes *Appl. Phys. Lett.* **100** 061107
[18] Biroju R K and Giri P K 2014 Defect enhanced efficient physical functionalization of graphene with gold nanoparticles probed by resonance Raman spectroscopy *J. Phys. Chem.* C **118** 13833
[19] Zhan Y, Liu Z, Najmaei S, Ajayan P M and Lou J 2012 Large-area vapor-phase growth and characterization of MoS_2 atomic layers on a SiO_2 substrate *Small* **8** 966
[20] Chow P K, Jacobs-Gedrim R B, Gao J, Lu T-M, Yu B, Terrones H and Koratkar N 2015 Defect-induced photoluminescence in monolayer semiconducting transition metal dichalcogenides *ACS Nano* **9** 1520
[21] Zhang Y, Li H, Wang H, Liu R, Zhang S and Qiu Z 2015 On valence-band splitting in layered MoS_2 *ACS Nano* **9** 8514
[22] Voiry D, Yang J and Chhowalla M 2016 Recent strategies for improving the catalytic activity of 2D TMD nanosheets toward the hydrogen evolution reaction *Adv. Mater.* **28** 6197
[23] Fabbri E, Habereder A, Waltar K, Kotz R and Schmidt T J 2014 Developments and perspectives of oxide-based

catalysts for the oxygen evolution reaction *Catal. Sci. Technol.* **4** 3800

[24] Yu Y, Huang S-Y, Li Y, Steinmann S N, Yang W and Cao L 2014 Layer-dependent electrocatalysis of MoS_2 for hydrogen evolution *Nano Lett.* **14** 553

[25] Pimenta M A, del Corro E, Carvalho B R, Fantini C and Malard L M 2015 Comparative study of Raman spectroscopy in graphene and MoS_2-type transition metal dichalcogenides *Acc. Chem. Res.* **48** 41

[26] Jae-Ung L, Kangwon K and Hyeonsik C 2015 Resonant Raman and photoluminescence spectra of suspended molybdenum disulfide *2D Mater.* **2** 044003

[27] Loan P T K, Zhang W, Lin C T, Wei K H, Li L J and Chen C H 2014 Graphene/MoS_2 heterostructures for ultrasensitive detection of DNA hybridisation *Adv. Mater.* **26** 4838

[28] Pierucci D *et al* 2016 Band alignment and minigaps in monolayer MoS_2-graphene van der Waals heterostructures *Nano Lett.* **16** 4054

[29] Conley H J, Wang B, Ziegler J I, Haglund R F, Pantelides S T and Bolotin K I 2013 Bandgap engineering of strained monolayer and bilayer MoS_2 *Nano Lett.* **13** 3626